analytical chemistry

Article

pubs.acs.org/ac

Carbon Nanotubes Grown on Metal Microelectrodes for the Detection of Dopamine

Cheng Yang,[†] Christopher B. Jacobs,[†] Michael D. Nguyen,[†] Mallikarjunarao Ganesana,[†] Alexander G. Zestos,[†] Ilia N. Ivanov,[‡] Alexander A. Puretzky,[‡] Christopher M. Rouleau,[‡] David B. Geohegan,[‡] and B. Jill Venton*[,†]

[†]Department of Chemistry, University of Virginia, McCormick Road, Box 400319, Charlottesville, Virginia 22904-4319, United States

[‡]Center for Nanophase Materials Sciences, Oak Ridge National Laboratory, 1 Bethel Valley Road, Building 8610, Oak Ridge, Tennessee 37831, United States

Supporting Information

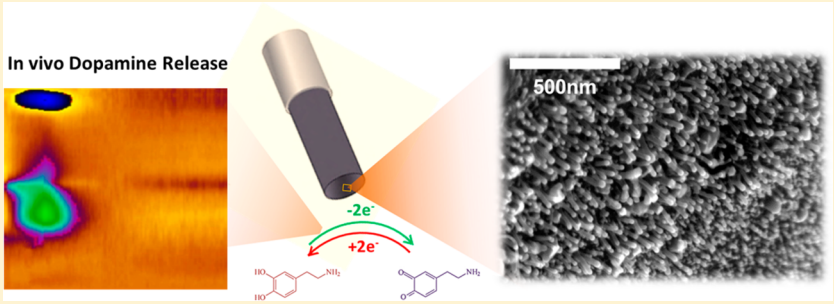

ABSTRACT: Microelectrodes modified with carbon nanotubes (CNTs) are useful for the detection of neurotransmitters because the CNTs enhance sensitivity and have electrocatalytic effects. CNTs can be grown on carbon fiber microelectrodes (CFMEs) but the intrinsic electrochemical activity of carbon fibers makes evaluating the effect of CNT enhancement difficult. Metal wires are highly conductive and many metals have no intrinsic electrochemical activity for dopamine, so we investigated CNTs grown on metal wires as microelectrodes for neurotransmitter detection. In this work, we successfully grew CNTs on niobium substrates for the first time. Instead of planar metal surfaces, metal wires with a diameter of only 25 μm were used as CNT substrates; these have potential in tissue applications due to their minimal tissue damage and high spatial resolution. Scanning electron microscopy shows that aligned CNTs are grown on metal wires after chemical vapor deposition. By use of fast-scan cyclic voltammetry, CNT-coated niobium (CNT-Nb) microelectrodes exhibit higher sensitivity and lower ΔE_p value compared to CNTs grown on carbon fibers or other metal wires. The limit of detection for dopamine at CNT-Nb microelectrodes is 11 ± 1 nM, which is approximately 2-fold lower than that of bare CFMEs. Adsorption processes were modeled with a Langmuir isotherm, and detection of other neurochemicals was also characterized, including ascorbic acid, 3,4-dihydroxyphenylacetic acid, serotonin, adenosine, and histamine. CNT-Nb microelectrodes were used to monitor stimulated dopamine release in anesthetized rats with high sensitivity. This study demonstrates that CNT-grown metal microelectrodes, especially CNTs grown on Nb microelectrodes, are useful for monitoring neurotransmitters.

Carbon nanotube (CNT)-modified electrodes have been widely used for the detection of biomolecules because of their unique properties including large active surface area, high conductivity, fast electron transfer kinetics, and biocompatibility.[1,2] These properties lead to reduced overpotential, minimal electrode fouling, and increased sensitivity and selectivity.[3,4] CNTs are especially attractive for making smaller electrodes because the high surface-area-to-volume ratio results in a large electroactive surface area for the adsorption of biomolecules.[5] A popular method to deposit CNT films onto microelectrodes is to dip carbon fiber microelectrodes (CFMEs) into CNT suspension or CNT/polymer composite solution.[6−9] However, CNTs are randomly distributed throughout the CNT films during the dip coating process. Therefore, most of the area exposed to the analyte solution is the sidewall of the CNTs, but the ends of the CNTs are more likely to be the most electrochemically active sites.[10−13] Moreover, large CNT agglomerations are easily formed, which cause high noise, and the cumbersome fabrication procedure reduces reproducibility.[7]

Previous studies have shown that vertically aligned CNTs on a microelectrode substrate are better for detecting neurotransmitters, such as dopamine.[14] One strategy is to chemically self-assemble vertically aligned CNTs on substrates with a solution deposition method. Our group developed single-walled carbon nanotube (SWCNT) forest-modified CFMEs for rapid

Received: April 2, 2015
Accepted: December 7, 2015
Published: December 7, 2015

DOI: 10.1021/acs.analchem.5b01257
Anal. Chem. 2016, 88, 645−652

and sensitive detection of neurotransmitters by use of fast-scan cyclic voltammetry (FSCV).[15] An alternative strategy is to directly grow CNTs in an aligned manner through chemical vapor deposition (CVD). Recently, Xiang et al.[16] used as-synthesized, vertically aligned carbon nanotube sheathed carbon fibers (VACNT-CFs) for the detection of dopamine and ascorbate in vivo. The VACNT-CFs microelectrodes exhibited promising electrochemical performance. However, since the carbon fiber is electrochemically active toward dopamine, the CF substrates limit studies of the properties of CNT coating. In comparison, metal substrates with CNT coating would have several benefits. First, although gold[17] and platinum[18] are active to dopamine, many other metals (e.g., Nb, Ta, Mo, W, Pd, Ti, and stainless steel used in this paper) lack electrochemical reactivity to dopamine, which enables the study of interaction of dopamine with CNTs without the convolution of possible substrate reactivity. Second, the inherently low conductivity of CF[10] may limit the overall conductivity of sensors, while metals have higher conductivity. Third, the electrochemical properties of the CF core vary with different waveforms and can affect the electrochemical properties.[19] Therefore, a metal substrate that lacks reactivity to dopamine and has high intrinsic conductivity and relatively stable electrochemistry may avoid these issues. Although successful growth of CNTs on several metal substrates has been reported,[20−26] CNTs have not been grown on niobium (Nb) substrates. In addition, all previous studies of CNT growth on metals have been on flat substrates and not on the cylindrical metal wires that would be needed for implantable electrochemical microsensors.

In this study, we explored the use of CNT-grown metal microelectrodes for enhanced neurotransmitter detection. The CNT-grown metal microelectrodes and CFMEs were fabricated by CVD and characterized by scanning electron microscopy (SEM) and Raman spectroscopy. These are the first studies to grow CNTs on Nb substrates or on small-diameter metal wires, instead of a planar metal surfaces such as foils, which allows them to be implanted in tissue with minimal damage and high spatial resolution.[27] CNTs grown on Nb were short and dense, and CNT-Nb microelectrodes exhibited better electrochemical response to dopamine via FSCV compared to CNTs grown on other metals or CFs. Moreover, the CNT-Nb microelectrodes were tested for electrochemical response to ascorbic acid, DOPAC (3,4-dihydroxyphenylacetic acid, a dopamine metabolite), serotonin, adenosine, and histamine. The CNT-Nb microelectrodes were used to detect stimulated dopamine release in anesthetized rats and exhibited high sensitivity with rapid measurements in vivo. Electrophysiology studies often use arrays of metal wires, and future experiments could investigate making arrays of the CNTs on metal wires for multiplexed electrochemical experiments.

EXPERIMENTAL SECTION

Synthesis of Carbon Nanotube-Coated Metal Wires and Carbon Fibers. Carbon fibers (T650-35, Cytec, Woodland Park, NJ) and metal wires including tantalum, niobium, molybdenum, tungsten, stainless steel, titanium, and palladium (diameter 0.001 in.; ESPI Metals, Ashland, OR) were used as electrode substrates. CNTs were grown in an aligned manner through CVD after a solid-phase catalyst was deposited on the substrate surface.[24,28] A thin film of Al_2O_3 (30 nm) followed by a film of Fe catalyst (1 nm) was deposited onto the metal wires (25 μm) or CFs (7 μm) by electron beam physical vapor deposition (Angstrom Engineering, Kitchener, Ontario, Canada). Since electron beam deposition is "line-of-sight" dependent, only one side of the substrate was coated with buffer layer and catalyst. As a result, the microelectrodes were half coated with CNT arrays. In a quartz tube CVD reactor, the Al_2O_3−Fe-coated CFs and metal wires were degassed in vacuum and the temperature of the reactor was slowly ramped up to 700 °C and held for 10 min with a flow mixture of Argon (2000 sccm) and H_2 (200 sccm). Then ethylene (10 sccm) was introduced through the quartz tube for 5 min to grow the CNTs.

Langmuir Isotherm Modeling. We used a Langmuir adsorption isotherm (eq 1) to model the adsorption and desorption process kinetics of dopamine:

$$\frac{\Gamma_{DA}}{\Gamma_s} = \frac{\beta_{DA} a_{DA}^b}{1 + \beta_{DA} a_{DA}^b} \quad (1)$$

Γ_{DA} is the amount of dopamine adsorbed on the electrode, Γ_s is the saturated amount of dopamine that can adsorb on the electrode, β_{DA} is the thermodynamic equilibrium constant (unitless) for dopamine, and a_{DA}^b is the activity of dopamine in bulk solution at equilibrium. The percent surface coverage, Γ_{DA}/Γ_s, can be expressed by the ratio of oxidation current of dopamine to theoretical saturated oxidation current, which is the plateau of the fitting curve. The activity is related to its molar concentration (C_{DA}) by eq 2:[29]

$$a_{DA} = (\gamma_{DA} C_{DA})(1\ \mathrm{L \cdot mol^{-1}}) \quad (2)$$

γ_{DA} is the activity coefficient of dopamine in bulk solution at the adsorption equilibrium. For a charged adsorbate solution at high concentration, the effect of the activity coefficients must be taken into account because charged adsorbates are governed by ionic interactions.[30] According to the Debye−Huckel law:

$$\log \gamma_{DA} = -Az^2 I^{1/2} \quad (3)$$

γ_{DA} is a function of ionic strength (I) of the solute and charge carried by each solute (z), while A is a constant that depends on temperature and is about 0.51 for water at 25 °C.[31] Thus, γ_{DA} for dopamine in phosphate-buffered saline (PBS) is 0.63 at room temperature.[32] β_{DA} can be used to calculate the adsorption Gibbs free energy of dopamine (eq 4):

$$\Delta \bar{G}^\circ_{DA} = -RT \ln \beta_{DA} \quad (4)$$

RESULTS AND DISCUSSION

Characterization of Carbon Nanotubes Grown on Metal Wires and Carbon Fibers. CVD allows direct growth of CNTs on substrates; however, no study had grown CNTs on Nb or on small-diameter cylindrical metal wires. We optimized CNT growth on metal wires for use as microelectrodes. Figure 1 shows SEM images of bare Nb (Figure 1A) and Ta (Figure 1B) wires as well as carbon fiber (Figure 1C) and the same substrates after CNT growth (Figure 1 D−F). The CNTs (multiwalled) grown on Nb are short, dense, and aligned, compared to the CNTs grown on Ta and CFs, which are longer and more randomly oriented. Since the end-caps of the CNTs would be open due to the applied voltage,[33] the ends would have more sp^3-hybridized, edge plane carbons that can be oxidized to provide functional groups.[10] The short, dense CNT bundles on the Nb would have more functionalized edge plane sites exposed compared to the more diffuse CNTs on CFs and Ta, where more sidewalls would be exposed to the analyte.

DOI: 10.1021/acs.analchem.5b01257
Anal. Chem. 2016, 88, 645−652

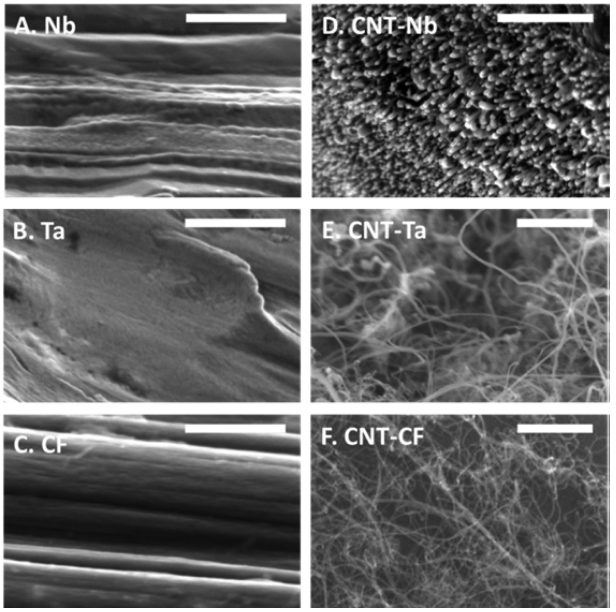

Figure 1. SEM images of (A) bare niobium, (B) bare tantalum, (C) bare CF, (D) CNT-grown niobium, (E) CNT-grown tantalum, and (F) CNT-grown CF. Scale bar: 500 nm.

The variety in CNT morphology grown on different metallic substrates might result from the interaction of Al_2O_3 buffer layer with the substrate or different properties of the metals. Al_2O_3 was used as a catalyst support buffer layer to enhance CNT growth by inhibiting diffusion of the catalyst material into the substrate upon heating.[34] However, the Al_2O_3 buffer layer has a different grain size on different substrates after heating, due to surface energy or wettability,[35−37] which leads to different CNT nucleation densities.[38] Another possible reason for the varied CNT morphology on different substrates is the amount of hydrogen absorbed in the metal substrates, which could affect the microstructure and mechanical properties of the resulting CNT gowth.[39] Among transition metals, group VB metals are good hydrogen storage substrates.[40−42] Therefore, the more aligned and consistent CNT growth on Nb and Ta might be due to hydrogen release that helps maintain the activation of iron catalysts.

To further characterize the CNT surface, Raman spectra of CNTs grown on metal wires and CF substrates were compared (Figure S1). The ratio of D/G peaks (D band originating from defects and G band from graphite) reveals the sp^3-hybridized content of the carbon film.[43] The D/G ratios (n = 5) for CNT-Nb, CNT-Ta, and CNT-CF are 2.2 ± 0.1, 1.8 ± 0.2, and 1.9 ± 0.6, respectively. The ratio of intensities of these peaks is often used as an indicator of the quality of CNTs, and these multiwalled CNTs are defect-rich.[44] The D/G ratio of CNTs grown on Nb is significantly larger than on Ta (unpaired t test, $p \leq 0.05$), which demonstrates CNTs on Nb are more defect-rich. The small standard errors observed indicate that the D/G ratio was consistent between electrodes.

Fast-Scan Cyclic Voltammetry of Dopamine at Bare Metal Wire and Carbon Fiber Microelectrodes. To investigate the electrochemical performance of the substrate materials, cylindrical microelectrodes were made of metal wires and carbon fibers. Figure 2A−C shows the background current measured in PBS at bare Nb, Ta, and CF electrodes with similar lengths (~70−100 μm). The capacitive currents arising from electrical double layer charging are small, around 300 nA for Nb and 100 nA for Ta metal wires. The square shape background for Nb and Ta metal wires reveals good polarizability.[10] In contrast, background currents at CFME can be attributed to surface functional groups as well as capacitive charging.[45]

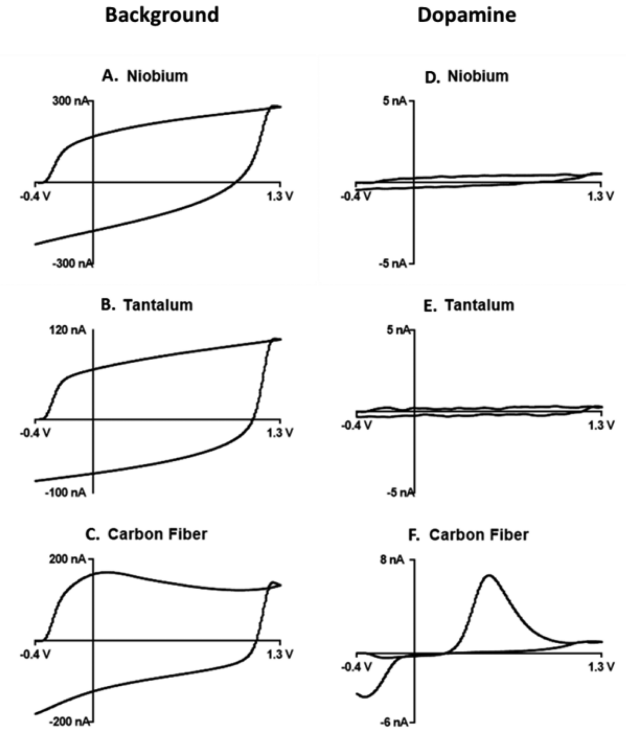

Figure 2. Electrochemical response of bare metal or carbon fibers with scan rate of 400 V/s and repetition frequency of 10 Hz. (Left) Background current in PBS solution for (A) niobium, (B) tantalum, and (C) carbon fiber microelectrodes. (Right) Background-subtracted cyclic voltammograms for 1 μM dopamine at bare (D) niobium, (E) tantalum, and (F) carbon fiber microelectrodes.

Figure 2D−F shows the background-subtracted cyclic voltammograms (CVs) of 1 μM dopamine at bare Nb, Ta, and CF microelectrodes. Nb and Ta are not electrochemically active for dopamine and show no Faradaic peaks. Therefore, any dopamine signal at CNT-Nb or CNT-Ta microelectrodes will arise from the CNTs. CFMEs have a robust signal for dopamine (Figure 2F) and are widely used as the standard electrode material in the field of in vivo voltammetry.

Fast-Scan Cyclic Voltammetry of Dopamine at Carbon Nanotube-Grown Metal Wire and Carbon Fiber Microelectrodes. Figure 3 shows the electrochemical response of CNT-grown Nb and Ta microelectrodes and CNT-grown CFMEs. The background charging currents for CNT-Nb and CNT-Ta electrodes (Figure 3A,B) are significantly larger than for the bare metals (Figure 2A,B), indicating substantial CNT growth. For CNTs grown on Nb and Ta wires, background-subtracted CVs for 1 μM dopamine (Figure 3D,E) show Faradaic peaks that were not present for bare wires (Figure 2D,E). Faradaic peaks for dopamine are also observed at CNT-CF microelectrodes, but the contribution of CNTs versus that of CF to the signal is harder to distinguish. Moreover, dopamine oxidation is more reversible at CNT-Nb microelectrodes than for CFMEs, which can be observed in the CVs.

Equilibration at carbon-based electrodes is required, since the carbon surface can change with application of the triangle waveform. Equilibration with a fast-scan triangle waveform (400 V/s, −0.4 to 1.3 V vs Ag/AgCl) mildly etches the carbon

DOI: 10.1021/acs.analchem.5b01257
Anal. Chem. 2016, 88, 645−652

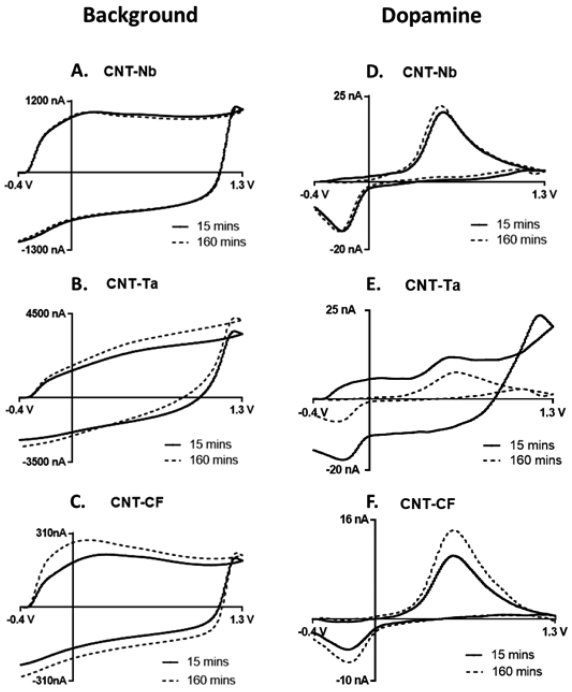

Figure 3. Comparison of electrochemical response at CNT-grown niobium, tantalum, and carbon fiber microelectrodes: background current at (A) CNT-Nb, (B) CNT-Ta, and (C) CNT-CF and background-subtracted cyclic voltammograms for 1 μM dopamine at (D) CNT-Nb, (E) CNT-Ta, and (F) CNT-CF microelectrodes. Measurements were taken after (—) 15 min and (---) 160 min of equilibration in PBS solution with a waveform of −0.4 to 1.3 V and back at 400 V/s, 10 Hz.

surface and introduces more oxygen-containing functional groups as active adsorption sites for dopamine.[45] For CNT-grown microelectrodes, the background (Figure 3A−C) and response to 1 μM dopamine (Figure 3D−F) were measured at two equilibration time points: waveform application for 15 and 160 min. Equilibration time mattered little for CNT-Nb microelectrodes, as the response to dopamine and background current were similar for both time points (Figure S2A). In contrast, CNT-Ta and CNT-CF required a longer equilibration time (Figure S2B,C). The shorter equilibration time might be due to abundant defect sites at CNT grown on Nb, which could be oxygen-functionalized faster by electrochemical activation.[46] The ends of CNTs grown on Nb are likely open, especially after continuous scanning with the 1.3 V triangle waveform, while the main sources of adsorption sites at CNT-Ta and CNT-CF are probably defects on sidewalls. The CNT-Nb microelectrode had no significant change in peak oxidative current for dopamine over 4 h, indicating the electrodes are stable over the typical time length of a biological experiment (Figure S3).

To compare the sensitivity of electrodes to dopamine, currents were corrected for surface area (based on their capacitive charging currents), since the metal wires are 25 μm in diameter while the CFME is 7 μm. As shown in Table 1, the current density at CNT-Nb microelectrodes for 1 μM dopamine is 197 ± 16 pA/μm^2, which is significantly larger than the current density at CNT-Ta, CNT-CF, or CFMEs [one-way analysis of variance (ANOVA) Bonferroni post-test, $p < 0.0005$, $n = 5$]. Current density at CFMEs after CNT growth is lower than that for bare CFMEs, indicating that much of

Table 1. Average ΔE_p, Current Density, and Limit of Detection for 1 μM Dopamine at Carbon Nanotube-Grown Microelectrodes and Carbon Fiber Microelectrode[a]

electrode	ΔE_p (V)	current density (pA/μm^2)	LOD (nM)
CNT-Nb	0.73 ± 0.03	197 ± 16	11 ± 1
CNT-Ta	0.87 ± 0.01	82 ± 10	91 ± 27
CNT-CF	0.81 ± 0.03	100 ± 25	46 ± 10
CFME	0.67 ± 0.01	135 ± 24	19 ± 4

[a]All $n = 5$; errors are standard error of the mean.

CNT grown on the CF substrate is not as electrochemically active as CF to dopamine. Because of the spaghettilike structure, not all of the CNTs on the CF may be available for electron transfer, but adding CNTs adds to the background current and noise. The limit of detection (LOD) is 11 ± 1 nM (S/N = 3) for dopamine at CNT-Nb microelectrodes, which is significantly lower than those at CNT-Ta, CNT-CF, and CFMEs (one-way ANOVA Bonferroni post-test, $p < 0.005$, $n = 5$). Therefore, with higher sensitivity and better LOD than CFMEs, CNT-Nb electrodes show promising electrochemical performance for dopamine detection.

Table 1 also gives the average values of oxidation and reduction peak separation of dopamine (ΔE_p) for CNT-grown metal wire microelectrodes and CFME. The ΔE_p values are significantly lower at CNT-Nb (one-way ANOVA Bonferroni post-test, $p < 0.01$, $n = 5$), yielding a peak separation that is ~140 and ~80 mV lower than those of CNT-Ta and CNT-CF microelectrodes, respectively. The smaller ΔE_p at CNT-Nb microelectrode might be caused by differing double-layer capacitances, uncompensated resistance, or ohmic drop.[5] However, because both the electrolyte and the size of the electrodes are similar, ohmic drop is an unlikely cause. Álvarez-Martos et al.[14] found that electron transfer was faster through oriented forestlike CNTs than nonoriented spaghettilike CNTs. The CNT-Nb morphology is denser and shorter than in CNT-Ta and CNT-CF, and the ends of the tubes are likely to have exposed defect sites for electron transfer. The mass transport per defect would be lower at CNT-Nb, based on the theory of charge transfer at partially blocked surfaces.[47] The larger number of active sites results in reduced diffusional flux per active site, which may also be the cause of smaller ΔE_p. In addition, there may be restricted mass transfer between the longer CNTs in spaghettilike CNT grown on Ta and CF. The overall ΔE_p at CNT-Nb microelectrodes is larger than at CFMEs, which shows that there are likely multiple factors affecting electron transfer, and the rate is also likely depressed by slow transfer through the Al_2O_3 buffer layer.

Characterization of Other Metal Substrates for Carbon Nanotube Growth. Other metal wires were tested for growing CNTs, including molybdenum (Mo), tungsten (W), palladium (Pd), stainless steel (SS), and titanium (Ti). Figure S4 shows the SEM images of both bare metals and CNT-grown metals. Larger CNT structures are apparent on W, Pd, SS, and Ti. On Pd, the carbon nanomaterial is larger in diameter and appears to be amorphous carbon, not CNTs. Moreover, CNTs grown on these metals are less dense than the CNTs grown on Nb, Ta, and CF. Background currents at these bare metal wires were approximately 3−10 times larger (Figure S5A−E) than at bare Nb and Ta microelectrodes (Figure 2A,B). None of the bare metals was electrochemically active toward dopamine (Figure S5F−J). After CNT growth, Mo, W, SS, and Ti do not have the typical characteristic peaks for

DOI: 10.1021/acs.analchem.5b01257
Anal. Chem. 2016, 88, 645−652

dopamine even after 160 min of equilibration (Figure S6). Carbon-coated Pd shows electrochemical activity to dopamine (Figure S6H), which is likely due to the amorphous carbon grown on Pd wires.

Our studies showed that the size of CNTs and the amount of growth depended on the metal substrate. CNT-Nb microelectrodes are preferred for neurotransmitter detection due to the short, dense, and vertically aligned CNT coating, which leads to high current density, low LOD, fast electron transfer rate, and short equilibration time. Thus, CNT-Nb microelectrodes were used for in vivo characterization studies.

Langmuir Isotherm Modeling. The redox reaction of dopamine at the surface of carbon-based sensors is an adsorption-controlled process.[48] Using a model for FSCV data developed by the Wightman group,[49] we previously determined that the adsorption/desorption kinetics of dopamine are different for CNT yarn electrodes than for CFMEs.[50] Here, we used a Langmuir adsorption isotherm to model the adsorption and desorption kinetics of dopamine at CNT-grown electrodes. The percent surface coverage is calculated from eq 1 and then the coverage versus concentration is fit with the Langmuir isotherm. The anodic peak (Figure 4) and the cathodic peak (Figure S7) give information about dopamine and dopamine-*o*-quinone (DOQ) adsorption, respectively.

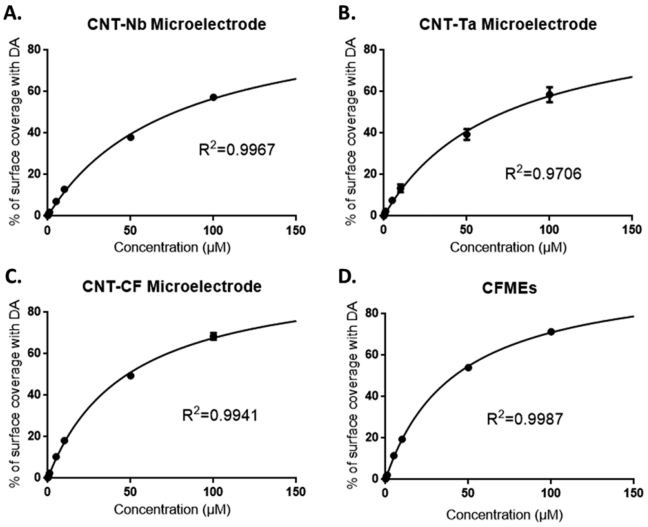

Figure 4. Plot of normalized anodic current to corresponding dopamine concentration. The fitting curve is modeled on the basis of eq 3, where C_{DA} is the *x*-axis and fractional surface coverage is the *y*-axis. An equilibrium value, β_{DA}, is fit for each curve. (A) CNT-coated Nb microelectrode; (B) CNT-coated Ta microelectrode; (C) CNT-coated CFME; (D) CFME (n = 5 per electrode material; error bar is standard error of mean and sometimes is so small as to be less than the size of the point).

Table 2 gives average adsorption rate constants for CNT-Nb, CNT-Ta, and CNT-CF microelectrodes as well as bare CFME. The β value is used to calculate the Gibbs free energy for dopamine and DOQ adsorption.

The adsorption equilibria for both dopamine (β_{DA}) and DOQ (β_{DOQ}) at CNT-Nb and CNT-Ta microelectrodes are smaller than those at CF and CNT-CF microelectrodes. This indicates dopamine and DOQ adsorb more strongly to CF and CNT-CF microelectrodes than to CNT-Nb and CNT-Ta microelectrodes. However, at the CNT-Ta and CNT-Nb microelectrodes, β_{DA} is similar to β_{DOQ}, and the ratio of β_{DA}/β_{DOQ} is about 1 (Table 2). At CFMEs, β_{DA} is significantly larger than β_{DOQ} (paired t test, $p < 0.005$, $n = 5$), and the β_{DA}/β_{DOQ} ratio is larger than at CNT-Nb microelectrodes (unpaired t test, $p < 0.05$, n = 5). Thus, DOQ is more likely to readsorb from the electrode at CNT-Nb, leading to a bigger reduction peak and more reversible reaction. The ratio of equilibrium constants for CNT-CF microelectrodes falls in between that of CFMEs and CNT-grown wires. The overall equilibrium is likely a convolution of the equilibrium at CNT-coated parts of the electrode and bare CFME, which is also partially exposed to solution. These data agree with previous modeling of CNT yarn electrodes, which showed differences in adsorption for dopamine and DOQ compared to CFMEs.[50]

Fast-Scan Cyclic Voltammetry of Other Neurochemicals. We tested the electrochemical performance of CNT-Nb microelectrodes toward the detection of other neurochemicals including ascorbic acid (AA), DOPAC (3,4-dihydroxyphenylacetic acid), serotonin, adenosine, and histamine. Since the detection of adenosine and histamine requires scanning to higher potentials, we used a waveform of −0.4 V to 1.45 V at 400 V/s.[51] Figure 5 shows sample CVs for each neurochemical (black solid line) compared to dopamine (red dashed line) at the same CNT-Nb electrode. The bar graphs compare the ratio of oxidation currents of the different neurotransmitters to dopamine at CNT-Nb microelectrodes and CFMEs.

Ascorbic acid is an anionic antioxidant present in high concentrations in the brain,[52] with a broad oxidation peak near the potential for dopamine detection (Figure 5A). The ratios of oxidative current for 200 μM AA to 1 μM dopamine at CNT-Nb microelectrodes are significantly smaller than those at CFMEs (Figure 5B, paired t test, $p < 0.0001$, $n = 5$), indicating CNT-Nb microelectrodes have better selectivity for dopamine over AA than CFMEs. Since AA is an anion at physiological pH,[53] the abundant oxygen-containing functional groups on the CNT surface might repel AA and further increase the selectivity for cationic dopamine. DOPAC is a dopamine metabolite[54] and has a similar oxidation potential to dopamine (Figure 5C). Although there is no significant difference in selectivity for dopamine over DOPAC at CNT-Nb microelectrodes (Figure 5D, paired t test, $p = 0.1454$, $n = 5$), the reduction potential of DOPAC is significantly more negative (−0.28 ± 0.01 V for

Table 2. Average Equilibrium Constants and Adsorption Gibbs Free Energy for Dopamine and Dopamine-*o*-quinone at Carbon Nanotube-Grown Microelectrodes and Carbon Fiber Microelectrode[a]

material	β_{DA} (×10³)	β_{DOQ} (×10³)	β_{DA}/β_{DOQ}	ΔG°_{DA} (kJ/mol)	ΔG°_{DOQ} (kJ/mol)	$\Delta G^{\circ}_{DA}/\Delta G^{\circ}_{DOQ}$
CNT-Nb	21 ± 1	20 ± 1	1.03 ± 0.04	−24.1 ± 0.1	−24.0 ± 0.1	1.003 ± 0.004
CNT-Ta	23 ± 3	23 ± 5	1.05 ± 0.09	−24.4 ± 0.3	−24.3 ± 0.4	1.003 ± 0.009
CNT-CF	37 ± 4	31 ± 2	1.10 ± 0.02	−25.6 ± 0.2	−25.1 ± 0.1	1.014 ± 0.005
CFME	39 ± 1	32 ± 1	1.23 ± 0.04	−25.9 ± 0.1	−25.2 ± 0.1	1.019 ± 0.003

[a]All n = 5. Errors are standard error of the mean.

DOI: 10.1021/acs.analchem.5b01257
Anal. Chem. 2016, 88, 645−652

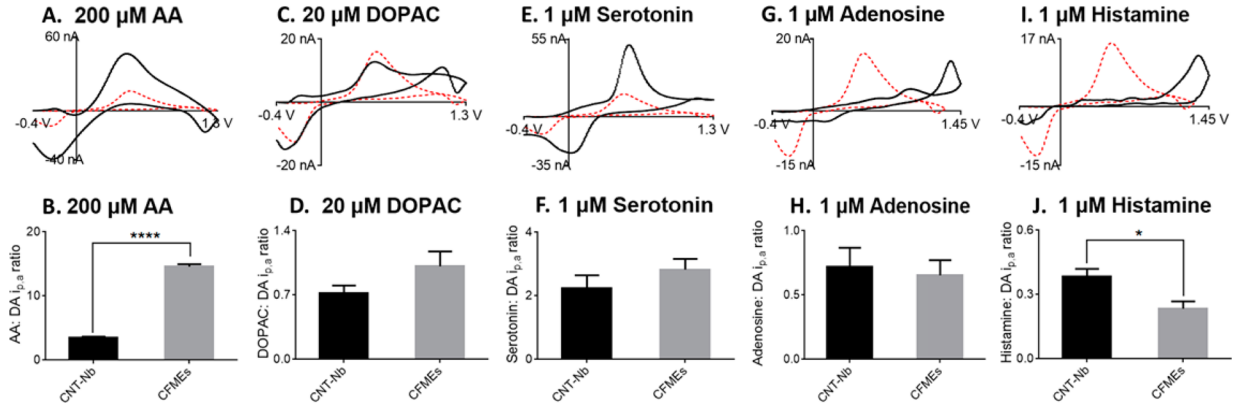

Figure 5. Detection of other neurochemicals at CNT-Nb microelectrodes. (Upper row) CVs of (A) 200 μM AA, (C) 20 μM DOPAC, (E) 1 μM serotonin, (G) 1 μM adenosine, and (I) 1 μM histamine in PBS buffer. Red dashed line is CV of 1 μM dopamine obtained from the same CNT-Nb electrode. For AA, DOPAC, and serotonin, the electrode was scanned to 1.3 V; for adenosine and histamine, the electrode was scanned to 1.45 V. (Lower row) Column plots show the ratio of oxidation current for (B) 200 μM AA, (D) 20 μM DOPAC, (F) 1 μM serotonin, (H) 1 μM adenosine, and (J) 1 μM histamine compared to the corresponding oxidation current of dopamine at CNT-Nb microelectrode (black, n = 5) and CFMEs (gray, n = 5). The oxidation current ratios at CNT-Nb microelectrodes are significantly different than CFMEs for the measurement of ascorbic acid (paired t test, $p < 0.0001$) and histamine (paired t test, $p < 0.05$).

DOPAC compared to −0.22 ± 0.01 V for dopamine; paired t test, $p < 0.001$, n = 5), similar to previous CNT electrode studies.[9] Serotonin is a cationic indolamine neurotransmitter.[55] The ratio of currents for serotonin to dopamine is similar for CNT-Nb microelectrodes and CFMEs (Figure 5F, paired t test, p = 0.3008, n = 5). The oxidation peak for serotonin is similar to that for dopamine as well, but the reduction peak is shifted by 200 mV (Figure 6E, paired t test, $p < 0.0001$, n = 5), which can be used to discriminate serotonin from dopamine. Adenosine is an important neuroprotective modulator in the brain that regulates neurotransmission and blood flow.[51] Adenosine is identified by its two oxidation peaks in the CV (a primary oxidation peak at 1.4 V and a secondary peak at 1.0 V; Figure 5G).[51] The selectivity for adenosine compared to dopamine at CNT-Nb microelectrodes is similar to that at CFMEs (Figure 5H, paired t test, p = 0.7476, n = 5). Histamine is a neurotransmitter that regulates sleep.[56] CNT-Nb electrodes have an oxidation peak near the switching potential (Figure 5I) and show significantly higher histamine to dopamine current ratios than CFMEs (Figure 5J, paired t test, $p < 0.05$, n = 5), which might be due to the better antifouling properties of the CNT surface toward histamine than CFMEs.[57] Overall, CNT-Nb microelectrodes are useful for detecting a variety of neurochemicals.

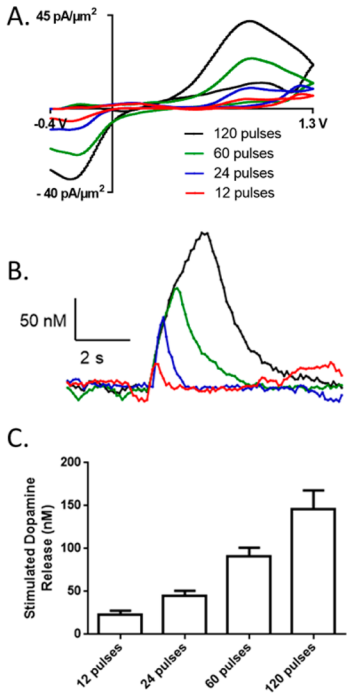

Figure 6. Dopamine detection in vivo at CNT-Nb microelectrodes. (A) Sample CVs depicting stimulated dopamine release detected from a CNT-Nb microelectrode placed in the caudate putamen with stimulation pulse trains of 120, 60, 24, and 12 pulses at 60 Hz. (B) Associated concentration vs time plot. (C) Averaged dopamine concentration at different pulses detected at CNT-Nb microelectrodes (n = 4). The electrode was scanned from −0.4 to 1.3 V and back at 400 V/s at 10 Hz.

In Vivo Detection of Dopamine at Carbon Nanotube-Grown Niobium Microelectrodes. To determine the applicability of the CNT-Nb microelectrode as a novel in vivo sensor, stimulated dopamine release was measured in anesthetized male Sprague-Dawley rats. Stimulation pulse trains were applied (300 μA, 12−120 pulses, 60 Hz) to the dopamine cell bodies, and the dopamine response was recorded in the caudate putamen near the terminals. Figure 6A,B show sample CVs and current versus time plots of dopamine detection at a CNT-Nb microelectrode with different stimulation pulses. Current increased as dopamine was released during the stimulation and decreased after the stimulation due to uptake.[52] Figure 6C gives the average dopamine concentration evoked in vivo; released dopamine is still detectable with as low as 12 stimulation pulses. The current density of the stimulated dopamine at CNT-Nb microelectrode in vivo [0.15 ± 0.02 pA/(nM·μm^2)] is slightly lower than that in vitro [0.20 ± 0.02 pA/(nM·μm^2)] but not significantly different (unpaired t test, $p >$ 0.05), which indicates CNT-Nb microelectrodes maintained relatively high sensitivity for in vivo dopamine detection. The CV of dopamine in vivo has a larger ΔE_p than that in vitro, likely due to adsorption of lipids, proteins, and peptides present in the extracellular fluid that slow electron transfer.[58,59] While the larger ΔE_p is not ideal, the sensitivity is maintained and the CV could be matched to in vivo spontaneous release. However,

DOI: 10.1021/acs.analchem.5b01257
Anal. Chem. 2016, 88, 645−652

future studies could focus on in vivo studies of protein fouling and adopt strategies that have been implemented for gold[60] and carbon fiber microelectrodes[61] to tune the surface adsorption of dopamine.

CONCLUSIONS

In summary, we successfully grew CNTs on Nb and used CNTs on cylindrical wires as microelectrodes for the first time. Small wire microelectrodes should minimize tissue damage and improve spatial resolution, which are needed for in vivo applications. This work is the first to compare CNT growth on various metal wires as well as carbon fibers, and the comparison is useful in choosing appropriate substrates for future CNT studies. CNTs forest-grown on Nb wires are shorter, denser, and more aligned than CNTs grown on other substrates, which led to enhanced current density and better LOD for dopamine. In addition, CNT-Nb microelectrodes are stable over 4 h of continuous measurement and are able to measure stimulated dopamine release in anesthetized rats. CNT-Nb microelectrodes have potential applications for the detection of neurotransmitters in vivo or metal electrode arrays in electrophysiology studies.

ASSOCIATED CONTENT

Supporting Information

The Supporting Information is available free of charge on the ACS Publications website at DOI: 10.1021/acs.analchem.5b01257.

Additional text describing solutions and microelectrode preparation, surface characterization, electrochemistry, in vivo measurements, and statistics; seven figures showing Raman spectra of CNTs grown on Nb, Ta, and CF, effect of electrochemical equilibration on CNT-metal microelectrodes, stability test on CNT-Nb microelectrodes, SEM images of bare and CNT-grown metal microwires, electrochemical response of bare metals, comparison of electrochemical response at CNT-grown metals and microelectrodes, and plot of normalized cathodic current to corresponding dopamine concentration fit with Langmuir isotherm (PDF)

AUTHOR INFORMATION

Corresponding Author

*E-mail jventon@virginia.edu; phone 434-243-2132.

Notes

The authors declare no competing financial interest.

ACKNOWLEDGMENTS

This research was supported by NIH Grant R21 DA037584. Synthesis and physical characterization of the CNT-metal wires were conducted at the Center for Nanophase Materials Sciences, which is a DOE Office of Science User Facility (User Grant CNMS2014-083).

REFERENCES

(1) Alwarappan, S.; Liu, G.; Li, C.-Z. *Nanomedicine* **2010**, *6* (1), 52–57.
(2) Tsierkezos, N. G.; Ritter, U. *J. Solid State Electrochem.* **2012**, *16* (6), 2217–2226.
(3) Salinas-Torres, D.; Huerta, F.; Montilla, F.; Morallón, E. *Electrochim. Acta* **2011**, *56* (5), 2464–2470.
(4) Habibi, B.; Jahanbakhshi, M.; Pournaghi-Azar, M. H. *Electrochim. Acta* **2011**, *56* (7), 2888–2894.
(5) Zestos, A. G.; Jacobs, C. B.; Trikantzopoulos, E.; Ross, A. E.; Venton, B. J. *Anal. Chem.* **2014**, *86*, 8568–8575.
(6) Swamy, B. E. K.; Venton, B. J. *Analyst* **2007**, *132* (9), 876–884.
(7) Jacobs, C. B.; Vickrey, T. L.; Venton, B. J. *Analyst* **2011**, *136* (17), 3557–3565.
(8) Zestos, A. G.; Nguyen, M. D.; Poe, B. L.; Jacobs, C. B.; Venton, B. J. *Sens. Actuators, B* **2013**, *182* (2013), 652–658.
(9) Peairs, M. J.; Ross, A. E.; Venton, B. J. *Anal. Methods* **2011**, *3* (10), 2379.
(10) McCreery, R. L. *Chem. Rev.* **2008**, *108* (7), 2646–2687.
(11) Jacobs, C. B.; Peairs, M. J.; Venton, B. J. *Anal. Chim. Acta* **2010**, *662* (2), 105–127.
(12) Liu, J. *Science (Washington, DC, U. S.)* **1998**, *280* (5367), 1253–1256.
(13) Yang, C.; Denno, M. E.; Pyakurel, P.; Venton, B. J. *Anal. Chim. Acta* **2015**, *887*, 17–37.
(14) Álvarez-Martos, I.; Fernández-Gavela, A.; Rodríguez-García, J.; Campos-Alfaraz, N.; García-Delgado, a. B.; Gómez-Plaza, D.; Costa-García, A.; Fernández-Abedul, M. T. *Sens. Actuators, B* **2014**, *192* (2014), 253–260.
(15) Xiao, N.; Venton, B. J. *Anal. Chem.* **2012**, *84* (18), 7816–7822.
(16) Xiang, L.; Yu, P.; Hao, J.; Zhang, M.; Zhu, L.; Dai, L.; Mao, L. *Anal. Chem.* **2014**, *86* (8), 3909–3914.
(17) Zachek, M. K.; Hermans, A.; Wightman, R. M.; McCarty, G. S. *J. Electroanal. Chem.* **2008**, *614* (1–2), 113–120.
(18) Ciszewski, A.; Milczarek, G. *Anal. Chem.* **1999**, *71* (5), 1055–1061.
(19) Swamy, B. E. K.; Venton, B. J. *Analyst* **2007**, *132* (9), 876–884.
(20) Delmas, M.; Pinault, M.; Patel, S.; Porterat, D.; Reynaud, C.; Mayne-L'Hermite, M. *Nanotechnology* **2012**, *23* (10), 105604.
(21) Atthipalli, G.; Epur, R.; Kumta, P. N.; Yang, M.; Lee, J.-K.; Gray, J. L. *J. Phys. Chem. C* **2011**, *115* (9), 3534–3538.
(22) Lepró, X.; Lima, M. D.; Baughman, R. H. *Carbon* **2010**, *48* (12), 3621–3627.
(23) Gao, L.; Peng, A.; Wang, Z. Y.; Zhang, H.; Shi, Z.; Gu, Z.; Cao, G.; Ding, B. *Solid State Commun.* **2008**, *146* (9–10), 380–383.
(24) Hiraoka, T.; Yamada, T.; Hata, K.; Futaba, D. N.; Kurachi, H.; Uemura, S.; Yumura, M.; Iijima, S. *J. Am. Chem. Soc.* **2006**, *128* (41), 13338–13339.
(25) Bayer, B. C.; Hofmann, S.; Castellarin-Cudia, C.; Blume, R.; Baehtz, C.; Esconjauregui, S.; Wirth, C. T.; Oliver, R. A.; Ducati, C.; Knop-Gericke, A.; Schlögl, R.; Goldoni, A.; Cepek, C.; Robertson, J. *J. Phys. Chem. C* **2011**, *115* (11), 4359–4369.
(26) Zestos, A. G.; Yang, C.; Jacobs, C. B.; Hensley, D.; Venton, B. J. *Analyst* **2015**, *140* (21), 7283–7292.
(27) Kozai, T. D. Y.; Jaquins-Gerstl, A. S.; Vazquez, A. L.; Michael, A. C.; Cui, X. T. *ACS Chem. Neurosci.* **2015**, *6* (1), 48–67.
(28) Tran, K. Y.; Heinrichs, B.; Colomer, J.-F.; Pirard, J.-P.; Lambert, S. *Appl. Catal., A* **2007**, *318* (2007), 63–69.
(29) Graham, D. *J. Phys. Chem.* **1953**, *57* (7), 665–669.
(30) Liu, Y. *J. Chem. Eng. Data* **2009**, *54* (7), 1981–1985.
(31) Archer, D. G.; Wang, P. *J. Phys. Chem. Ref. Data* **1990**, *19* (2), 371.
(32) Mortimer, R. G. *Physical Chemistry*, 3rd ed.; Academic Press: San Diego, CA, 2008.
(33) Holloway, A. F.; Toghill, K.; Wildgoose, G. G.; Compton, R. G.; Ward, M. a H.; Tobias, G.; Llewellyn, S. a; Ballesteros, B.; Green, M. L. H.; Crossley, A. *J. Phys. Chem. C* **2008**, *112* (28), 10389–10397.
(34) Magrez, A.; Seo, J.; Smajda, R.; Mionić, M.; Forró, L. *Materials* **2010**, *3*, 4871–4891.
(35) Matthews, K. D.; Lemaitre, M. G.; Kim, T.; Chen, H.; Shim, M.; Zuo, J.-M. *J. Appl. Phys.* **2006**, *100* (4), 044309.
(36) Delzeit, L.; Nguyen, C. V.; Chen, B.; Stevens, R.; Cassell, A.; Han, J.; Meyyappan, M. *J. Phys. Chem. B* **2002**, *106*, 5629–5635.
(37) Parthangal, P. M.; Cavicchi, R. E.; Zachariah, M. R. *Nanotechnology* **2007**, *18* (18), 185605.

DOI: 10.1021/acs.analchem.5b01257
Anal. Chem. 2016, 88, 645–652

(38) Burt, D. P.; Whyte, W. M.; Weaver, J. M. R.; Glidle, A.; Edgeworth, J. P.; Macpherson, J. V.; Dobson, P. S. *J. Phys. Chem. C* **2009**, *113* (34), 15133−15139.
(39) Raney, J. R.; Misra, A.; Daraio, C. *Carbon* **2011**, *49* (11), 3631−3638.
(40) Uehara, I.; Sakai, T.; Ishikawa, H.; Takenaka, H. *Corrosion* **1989**, *45* (7), 548−553.
(41) Lewis, F. A. *Pure Appl. Chem.* **1990**, *62* (11), 2091−2096.
(42) Davenport, J.; Dienes, G.; Johnson, R. *Phys. Rev. B: Condens. Matter Mater. Phys.* **1982**, *25* (4), No. 2165.
(43) Filik, J.; May, P. W.; Pearce, S. R. J.; Wild, R. K.; Hallam, K. R. *Diamond Relat. Mater.* **2003**, *12* (3−7), 974−978.
(44) Feng, X.; Liu, K.; Xie, X.; Zhou, R.; Zhang, L.; Li, Q.; Fan, S.; Jiang, K. *J. Phys. Chem. C* **2009**, *113* (22), 9623−9631.
(45) Takmakov, P.; Zachek, M. K.; Keithley, R. B.; Walsh, P. L.; Donley, C.; McCarty, G. S.; Wightman, R. M. *Anal. Chem.* **2010**, *82* (5), 2020−2028.
(46) Miller, T. S.; Macpherson, J. V.; Unwin, P. R. *Phys. Chem. Chem. Phys.* **2014**, *16* (21), 9966.
(47) Amatore, C.; Savéant, J. M.; Tessier, D. *J. Electroanal. Chem. Interfacial Electrochem.* **1983**, *147* (1−2), 39−51.
(48) Atcherley, C. W.; Laude, N. D.; Parent, K. L.; Heien, M. L. *Langmuir* **2013**, *29* (48), 14885−14892.
(49) Bath, B. D.; Michael, D. J.; Trafton, B. J.; Joseph, J. D.; Runnels, P. L.; Wightman, R. M. *Anal. Chem.* **2000**, *72* (24), 5994−6002.
(50) Jacobs, C. B.; Ivanov, I. N.; Nguyen, M. D.; Zestos, A. G.; Venton, B. J. *Anal. Chem.* **2014**, *86* (12), 5721−5727.
(51) Nguyen, M. D.; Lee, S. T.; Ross, A. E.; Ryals, M.; Choudhry, V. I.; Venton, B. J. *PLoS One* **2014**, *9* (1), e87165.
(52) Robinson, D. L.; Venton, B. J.; Heien, M. L. A. V.; Wightman, R. M. *Clin. Chem.* **2003**, *49* (10), 1763−1773.
(53) Pisoschi, A. M.; Pop, A.; Serban, A. I.; Fafaneata, C. *Electrochim. Acta* **2014**, *121*, 443−460.
(54) Huffman, M. L.; Venton, B. J. *Electroanalysis* **2008**, *20* (22), 2422−2428.
(55) Baur, J. E.; Kristensen, E. W.; May, L. J.; Wiedemann, D. J.; Wightman, R. M. *Anal. Chem.* **1988**, *60* (13), 1268−1272.
(56) Robinson, D. L.; Hermans, A.; Seipel, A. T.; Wightman, R. M. *Chem. Rev.* **2008**, *108* (7), 2554−2584.
(57) Ross, A. E.; Venton, B. J. *Analyst* **2012**, *137* (13), 3045−3051.
(58) Chandra, S.; Miller, A. D.; Bendavid, A.; Martin, P. J.; Wong, D. K. Y. *Anal. Chem.* **2014**, *86* (5), 2443−2450.
(59) Park, J.; Show, Y.; Quaiserova, V.; Galligan, J. J.; Fink, G. D.; Swain, G. M. *J. Electroanal. Chem.* **2005**, *583* (1), 56−68.
(60) Chen, C.-H.; Luo, S.-C. *ACS Appl. Mater. Interfaces* **2015**, *7* (39), 21931−21938.
(61) Singh, Y. S.; Sawarynski, L. E.; Dabiri, P. D.; Choi, W. R.; Andrews, A. M. *Anal. Chem.* **2011**, *83* (17), 6658−6666.

DOI: 10.1021/acs.analchem.5b01257
Anal. Chem. 2016, 88, 645−652